

Effect of surface energy on nucleus morphology in heterogeneous ice nucleation

Pengfei Wang,^{1,2} Jun Zhang,^{1*} Hui Gao,^{1,2} Guice Yao¹ and Dongsheng Wen,^{1,3*}

¹⁾*School of Aeronautic Science and Engineering, Beihang University, Beijing 100191, China*

²⁾*Beihang Hangzhou Innovation Institute Yuhang, Beihang University, Xixi Octagon City, Yuhang District, Hangzhou 310023, China*

³⁾*Institute of Thermodynamics, Technical University of Munich, Munich, Germany*

(*Email: d.wen@buaa.edu.cn)

(*Email: jun.zhang@buaa.edu.cn)

Abstract: Icing on solid surfaces severely threatens safety and functioning of various engineering applications. The morphology of ice nucleus is of both practical meaning for ice control method and theoretical importance for nucleation theory, which however is still lack of clear understanding. This paper for the first time realizes a direct investigation of nucleus morphology in molecular dynamics (MD) simulations via a new identification algorithm, which enables us to visualize nucleus growth morphologies under different surface energies. Three morphology patterns, i.e., cubic, hex and mixed form, are discovered and explained by underlying nucleation pathways decided by the strength of surface energy only. The influence of initial morphology on the nucleation kinetics is for the first time investigated by the Seed method, which however shows no influence on subsequent growth speed and has only limited influence on subsequent morphology evolution. The effect of surface energy is found to be the key factor deciding nucleus morphology in heterogeneous nucleation. The new identification algorithm of ice nucleus, and the revelation of surface energy dependent morphological patterns and nucleation pathways are of great implications for understanding ice morphological behaviors in larger scales.

Keywords: Nucleation, nucleus, molecular simulation, icing, nucleation kinetics

I. INTRODUCTION

Icing phenomena are prevalent in all scales and various applications, including polar caps icing affecting global climate^{1,2}, turbine³ or wing icing leading to aircraft crashing⁴⁻⁷ or power network collapse⁸⁻¹⁰, droplet icing in heat ex-changer devices and molecule icing in stem cell and tissue storage^{11,12}. In most cases, heterogeneous nucleation that mediated by minute foreign particles is the dominant mechanism of ice formation^{13,14} in contrast to homogeneous nucleation of pure water freezing in the absence of foreign agents, for the reason that heterogeneous nucleation facilitates icing procedures and enables its occurrence under natural environment^{13,15}. Therefore, understanding conditions and mechanism of heterogeneous nucleation will be of great benefit to mediate/prevent ice formation in various situations¹⁵⁻¹⁷. Thus, investigating how surface conditions (material properties) initiate and influence heterogeneous icing is the major research approach at present^{15,18-20}.

Among various effects influencing heterogeneous nucleation, surface wettability or surface energy of foreign materials as an anticipatable and controllable perceptual property²¹ is highlighted in previous science studies of water phase change and has accumulated noticeable results in its effect on nucleation barrier, nucleation rates²²⁻²⁵ and other kinetic behaviors of heterogeneous nucleation²⁶⁻²⁸. Nonetheless, surface energy effect on nucleus morphology has been largely neglected, whose influence is still unclear.

Nucleus shape or morphology²⁹ as a visually intuitive research dimension, influences all research aspects from theoretical investigations^{30,31} to practical applications. Nucleus

morphology not only underlies the nucleation pathway of lowest energy barrier^{27,32}, but also indicates the difficulties to remove it off the surface through certain de-icing techniques^{9,33,34}. On one hand, the morphology of ice nucleus determines the configuration of water-ice surface and decides the energy barrier brought by water-ice interfacial energy^{35,36}. Ice nucleus is assumed as spherical in most prevalent molecular dynamics (MD) simulation researches²²⁻²⁴, however, the morphology of solid state in phase transition theory is assumed with certain geometrical shapes³⁵⁻⁴⁰ and non-spherical shapes, which have been proved existing by both experimental⁴¹⁻⁴⁴ and simulation studies^{45,46}. Investigation into nucleus morphology is of high theoretical importance. On the other hand, nucleus morphology of smaller contact area with solid and removable structures is preferred in de-icing applications^{9,33,34}. Concluding different ice morphologies will profoundly benefit our construction of universal nucleation theory and design of prevent/de-icing techniques. Yet morphological investigations are seldom mentioned in relevant researches, seldom is known as to morphological transformation under different surface energies²⁹.

A major challenge faced by researchers to explore nucleus morphology is the limitation from the length scale and timescale²⁹. Nucleus that could sustain spontaneous growth generally consist of hundreds to thousands of water molecules and only exist for several picoseconds, the scale of which is far beyond the reach of normal detection techniques⁴⁷⁻⁴⁹ and macroscopic simulation method^{50,51}. An alternative to capture crystal morphology during nucleation is to use highly accurate molecular simulations with a long-tested tool such as molecular dynamics (MD)⁵². Numer-

ous MD simulations have explored the spatial and temporal evolution of heterogeneous ice nucleation in many research dimensions^{22–24,27,32}, but the ice identification method, which distinguishes ice molecules from normal water molecules, is not precise enough to trace the nucleus shape^{53,54}. The considerable amount of identified quasi-ice molecules greatly clouded our judgement of cluster morphology and prohibited us from straightforward monitoring morphology evolutions in MD simulations⁵⁵.

This paper proposes an improved identification method for nucleus morphology studies in MD simulations and investigates the surface energy effect on crystal morphology. The proposed algorithm in Sec. II enables direct observation of the evolution of ice crystal morphology in nucleation and following investigations into parameters that influence ice morphology. In Sec. III A, we discover that ice cubic (Ic) and ice hex (Ih) structures of nucleus in MD simulations exhibit different morphologies akin to macroscopic ice shapes like hexagonal prisms from hex cell and tetrahedrons from cubic cell. In Sec. III B we conclude three distinct morphological patterns and their possible nucleation pathways under different surface energies. A spontaneous promotion of Ic structures by increasing nucleus size is discovered from similarities in different nucleation pathways. Divergence of nucleation pathways shows a suppression of Ic structures under stronger surface energy, directing nucleus into different pathways leading to different morphological patterns concluded. In Sec. III C the influence of pristine morphology and surface effect on subsequent nucleation pathways are analyzed in detail. Pristine morphology is proved of limited effect on subsequent nucleation process. Surface energy decides the ultimate nucleus morphology and growth rate. The new identification algorithm specialized in this paper is meaningful for future researches on nucleus morphology using MD method. Surface energy effect discovered on nucleus morphology in heterogeneous nucleation is fundamental to understand ice morphological behaviors in larger scales.

II. METHOD

A. Identification method

There exists principal incompetence in present identification method like Frenkel method⁵⁶ and CHILL+ method⁵⁴ for ice identification under certain simulation scenarios. The fundamental philosophy adopted by these methods to identify crystal molecules is that molecules in same lattice structure should possess same spatial correlation and consequently present certain identical characteristic properties which liquid molecules do not have⁵³. Identification method in MD simulations all follows this principle and use order parameters as such features to distinguish ice from water by designing certain algorithms.

$$\mathbf{q}_l = \{q_{-lm}, q_{(-l+1)m}, \dots, q_{(l-1)m}, q_{lm}\} \quad (1)$$

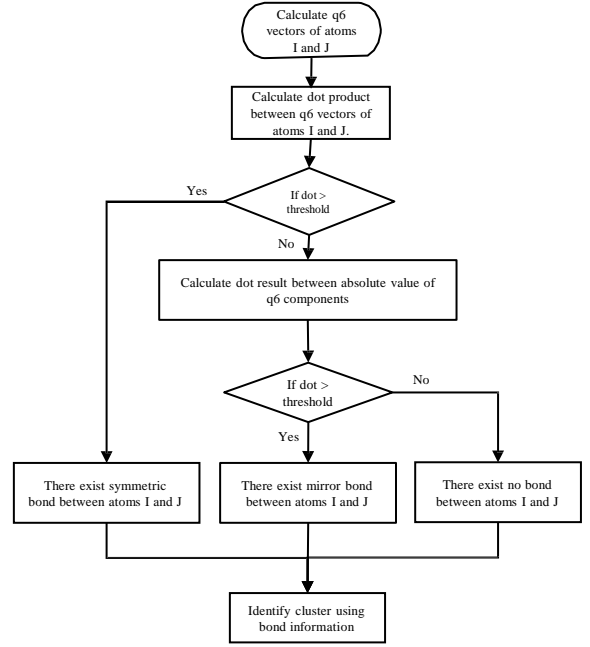


FIG. 1. New algorithm proposed by this paper.

$$q_{lm} = \frac{1}{N_b} \sum_{\text{bonds}} Q_{lm}(\mathbf{r}) \quad (2)$$

$$l=6 \quad m = -l, -l+1, \dots, l-1, l$$

$$\mathbf{q}_6(i) \cdot \mathbf{q}_6(j) = \frac{\sum_{m=-6}^6 q_{6m}(i) \cdot q_{6m}^*(j)}{|\sum_m q_{6m}(i)| |\sum_m q_{6m}(j)|} \quad (3)$$

The most widely adopted Steinhardt order parameter and its composing vectors in Eqn (1) and Eqn (2) represent the calculated molecule's spatial relationship. When two molecules i and j have similar lattice structures, their spatial vectors (q_6 vectors, see Eqn (3)) should resemble each other, which means that dot product of normalized vector should be close to 1. The original Frenkel method sets a threshold near 1 to decide if crystalline structures exist between identified pair of water molecules. Once the calculated normalized dot product between objected molecules i and j larger than threshold, Frenkel method considers these two molecules are both ice molecules and connected with a virtual solid bond⁵⁶. However, there exists two types of symmetry of cubic ice and hex ice in icing MD simulation results. Such ideal design of algorithms could only apply to bonds of central symmetry around its midpoint like purple bonds marked in Fig. 3(a) but fail to identify bonds of mirror symmetry like hexagonal ice, i.e., yellow bonds in marked in Fig. 3(a). Researchers employ such a method always supplement its results with the neighboring molecules around identified clusters as quasi-ice molecules^{22–24}, which brings big ambiguity in tracing crystal boundary and incompetence to investigate nucleus morphology as Fig. 2(a) shows. Other researchers created CHILL+

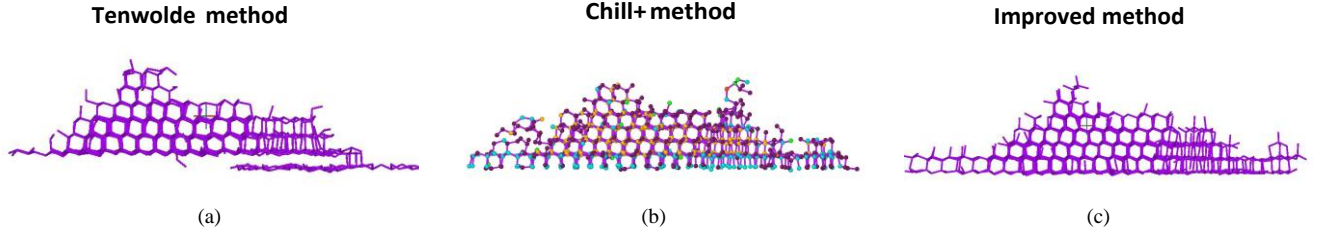


FIG. 2. Comparison of different identification method. (a) Result of original Frenkel method with no quasi-ice molecules. (b) Result of CHILL+ method. (c) Result of new method of this paper.

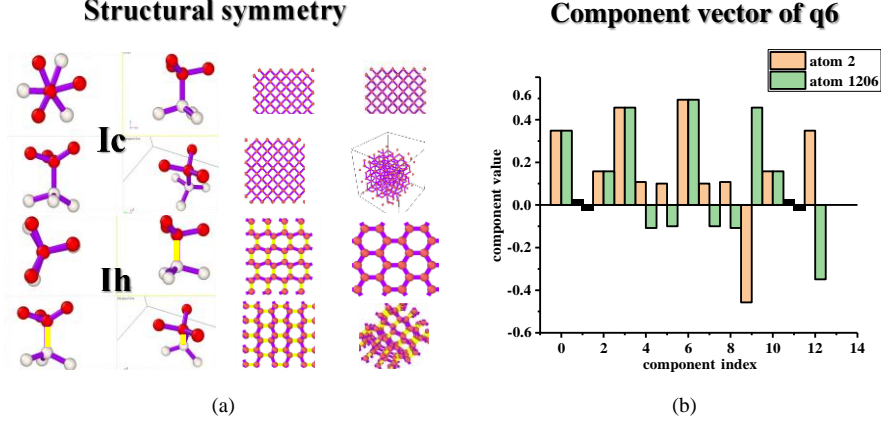


FIG. 3. (a) Identification result of standard Ih and Ic structures with Frenkel Method. Purple bonds are identified bonds, yellow bonds are missed bonds. (b) Components of $q_6(i)$ and $q_6(j)$ between a mirror bond. We could discover that signs of these two vectors are opposite in certain dimensions.

method using q_3 vector to include molecules of different symmetry by dividing dot product output into different regions to represent different symmetric bond structure as eclipse bond and staggered bond⁵⁴. But such a method does not work well for molecules on the surface as Fig. 2(b) shows, which deprives it of ability to discover pristine nucleus induced by surface at first time.

To investigate heterogeneity effect on nucleus morphology, we design an improved identification algorithm using q_6 vector which performs well for morphological studies of nucleus grown on the surface. The improved algorithm utilizes statistical features of q_6 and construct clusters solely by bond relationship identified. As hexagonal ice (Ih) and cubic ice (Ic) are most prevalent in MD icing simulations, after systematically examining effectiveness of the Frenkel method using standard hexagonal ice (Ih) and cubic ice (Ic) structures, we found the incapability of identification only exists in identification of axis bond in Ih structures as the yellow bonds in Fig. 3(a) shows (purple bonds are successfully identified with Frenkel method). Reason for such malfunction is the difference in symmetry causing different signs in q_6 vectors between identified pair of molecules. The molecules connected with axis bond are of mirror symmetry about the bond instead of center symmetry like all other identified bonds as Fig. 3(a) indicates. We discover that by manually identifying inverse the sign of vector component, the result of dot product could

still be close to 1. Utilizing such statistical features could not only supplement the omissive bonds but also distinguish Ih and Ic structures using this bond. Furthermore, elimination of neighboring quasi-ice molecules could also be achieved in identification of clusters by solely using bond relations identified. Namely, if one molecule is not connected with bond to the target cluster, it should not be regarded as part of the cluster.

After full examination and analysis of Frenkel method, our new algorithm to identify ice nucleus in MD simulation results is as Fig. 1 shows. The new algorithm designed is capable of giving a clear description of water-ice boundary and differentiating Ih/Ic structures through different symmetries as compared in Fig. II A, which enables subsequent morphological investigations and constitution analysis into nucleation process.

B. Simulation system

We choose graphite surface as substrate to simulate the nucleation of ice with water-carbon interactions that reproduce the experimental contact angle for water on graphite⁵⁷. As Fig. II B illustrates, simulation cell is composed of graphene layer, water film and vacuum regions. Single layer graphene surface of 10.3nm*10.3nm is constructed by VMD software⁵⁸

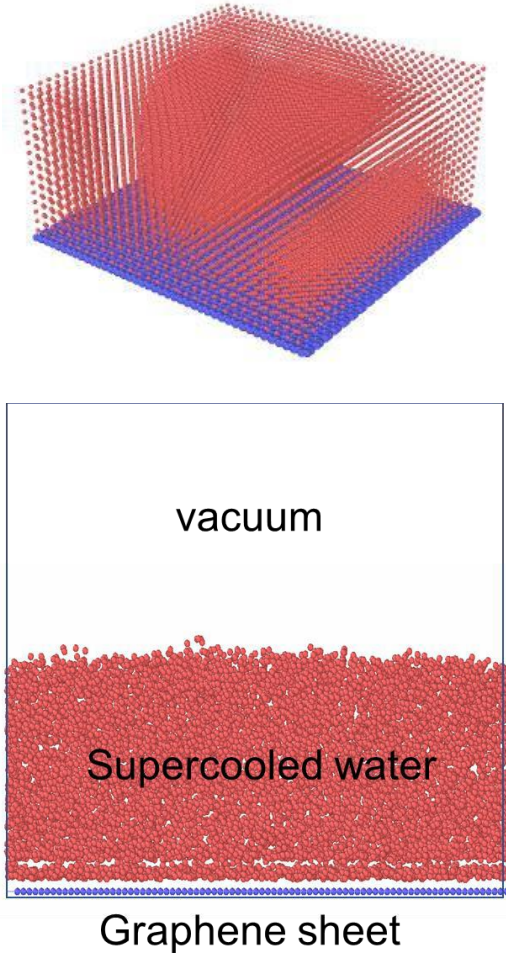
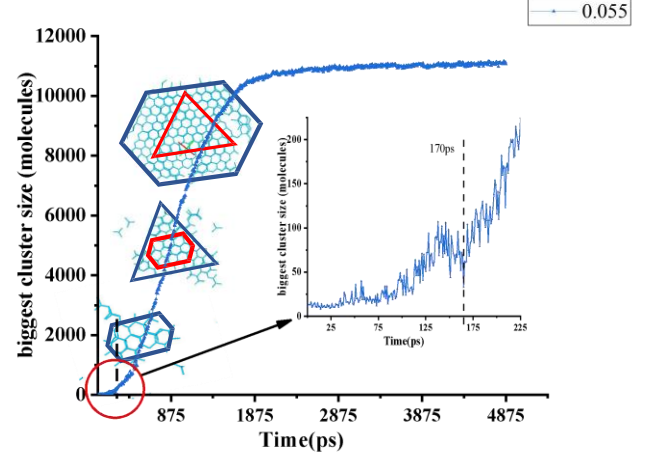


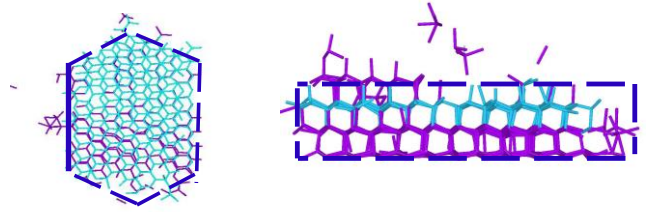
FIG. 4. Simulation system setting.

, with 3864 carbon atoms and periodic boundary conditions in x and y direction. Water film contains 12180 water molecules with 4 nm height. Height of vacuum region is 3 nm.

Interactions between water molecules are depicted with mW water potential model⁵⁹. The mW water model does not have hydrogen atoms and charges and treat water molecule as a coarse-grained particle, using three-body nonbonded interactions to form tetrahedral “hydrogen-bonded” structures⁵⁹. The interactions between mW water molecules is the summation of pairwise and three-body contributions described by the functional form of the Stillinger Weber (SW) potential⁶⁰. The interaction between water and carbon in the graphitic surfaces is described by a two-body SW potential, where the size and strength of the water carbon interaction parameters have been tuned in order to obtain the experimental contact angle for graphite, 86°^{61,62}. The contact angle was determined following the procedures of Ref⁵⁷. The interaction of water with the rough hydrophobic surface is also represented by a two-body SW potential characterized by $\sigma_{WC} = 0.32nm$, $\epsilon_{WC} = 0.0056 eV$ ⁵⁷. The equations of motion of the atoms of the graphitic surfaces are not integrated (i.e., they are fixed), therefore, there is no need to define carbon-carbon interaction poten-



(a) Size of biggest nucleus in simulations in nucleation process and nucleus shape under 0.0056 eV.



(b) Ih prism morphology, purple part is Ih structure while blue part is Ic structure.

FIG. 5. Illustration of Ih morphology.

tials.

$$\text{cubicity} = \frac{N_{\text{cubic}}}{N_{\text{cubic}} + N_{\text{hex}}} \quad (4)$$

Molecular dynamic procedure is implemented with LAMMPS software⁵² using a timestep of 5fs and integration algorithm of VERLET algorithm⁶³. Water molecules are given a temperature of 300K initially and relaxed with nose-hoover algorithm⁶⁴ by NVT ensemble. Then, temperature of water film are controlled down to 200K in 0.1 nanoseconds and relaxed for 5 nanoseconds afterwards to observe nucleation phenomenon⁵⁷. After tests, the initiation time for nucleation is too long when water-carbon potential is smaller than 0.0025 eV (contact angle about 124.9525 degrees, hydrophobic) while too fast when water-carbon potential larger than 0.009 eV (contact angle about 31.671 degrees, hydrophilic). So, we choose [0.2, 1.0] as our testing range to change the strength of water-carbon surface energy. The cubicity calculated in this paper is the portion of cubic ice in an integrated nucleus as Eqn. 4 shows. To eliminate randomness, simulation under each potential is restarted for 50 times using different initial speed seeds.

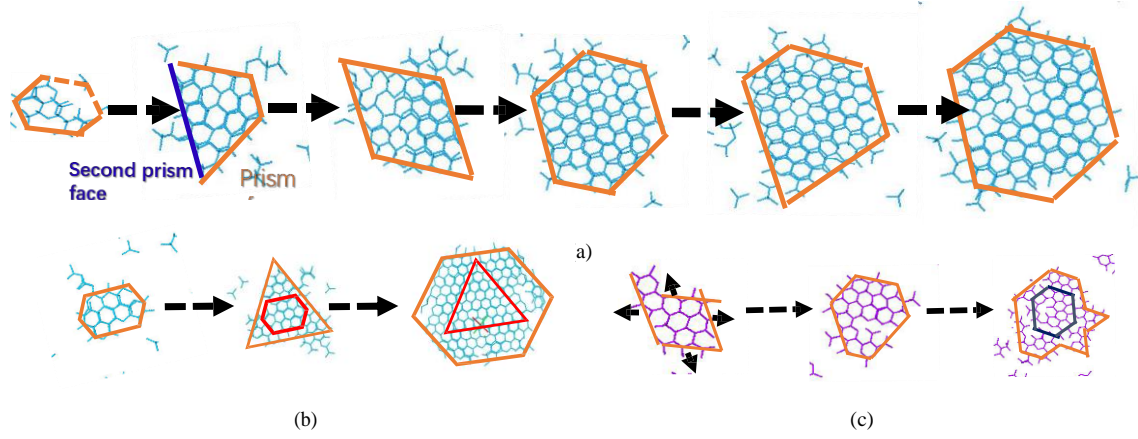


FIG. 6. Ih morphology sliced under 0.0045 eV, 0.0056 eV and 0.009 eV.

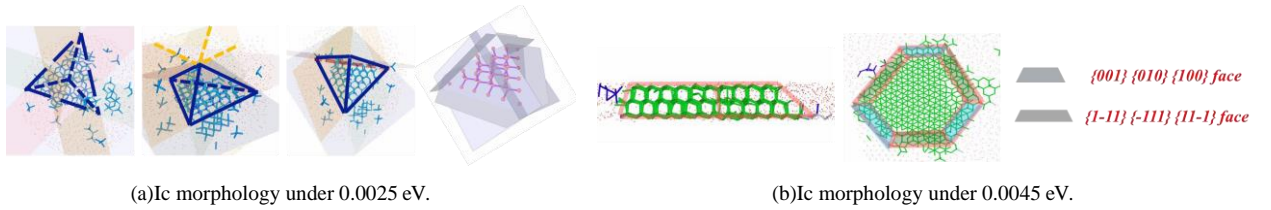


FIG. 7. Illustration of different Ic morphologies under 0.0025 and 0.0045 eV.

III. RESULTS AND DISCUSSION

A. Morphologies of Ih and Ic constituents in nucleus growth

Extraction of Ih and Ic structure from our simulation results suggests that both Ih and Ic structures in the nucleus tend to exhibit morphology kin to macroscopic ice shapes like hexagonal prisms from hex cell and tetrahedrons from cubic cell. Ih and Ic structures appear alternatively in sandwich structure (Fig. 8(a)) by transforming into each other's structure through equivalent crystal face brought by structural similarity.

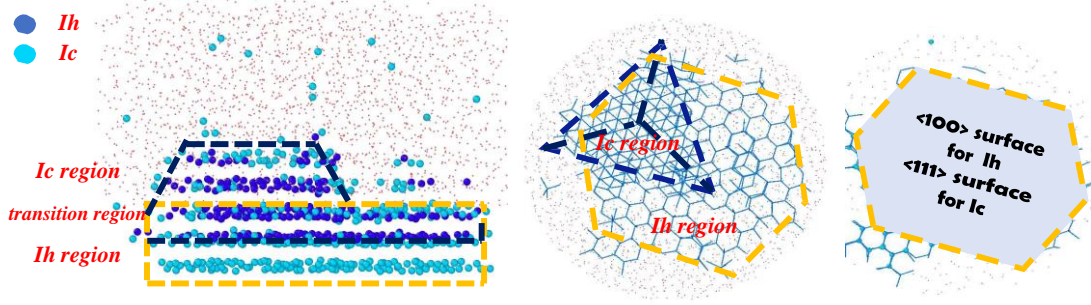
1. Morphologies of Ih and Ic in nucleus grow

Ih structures tend to arise on the graphite surface and exhibit regular prism structures on the whole as Fig. 5(b) shows, which accord well with all crystal faces in standard hexagonal ice structures and facilitate us to use shape of contact region to represent the integrate morphology of Ih. Variation of contact region with growth of nucleus size in the case of surface energy $\epsilon = 0.56$ eV is illustrated in Fig. 5(a), shape of other cases is shown in Fig. 6. Different from macroscopic observations of standard hexagonal geometry consisting of major prism face of hexagonal ice, second prism face may also emerge in microscopic nucleus shapes or bring out trapezoid geometries as transitional state between hexagonal shapes as marked in Fig. 6(a). All six counterparts of prism face may also not emerge at the same point which produces triangular or rhomboid patterns in the process of hexagonal shape

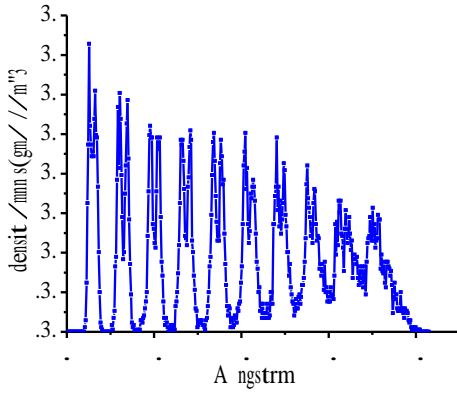
expanding, as randomness in microscope complicate the synchronization of surface propagation.

Ic structures are stacked on the basal face of Ih structures as Fig. 8(a) illustrates. The integral shape of Ic structures exhibits morphology of tetrahedron (Fig. 7(b)) or oblique prismoid (Fig. 7(b)), enclosed by $\{001\}$ face and its counterparts or $\{111\}$ face and its counterparts. Primitive Ic structure is in the shape of tetrahedron. In the process of tetrahedron expanding itself during its growth, it gradually produces other faces of $\{111\}$ face and its counterparts and introduces the shape of oblique prismoid. The emergence of $\{100\}$ comes much later than $\{111\}$ face in Ic structures.

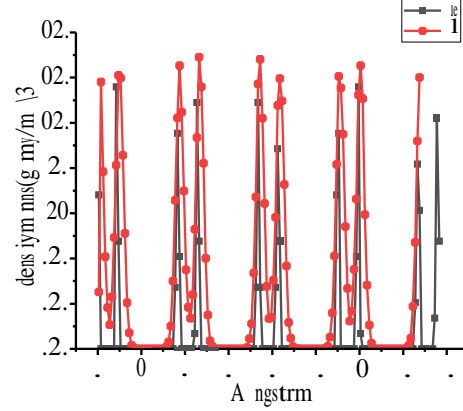
Shape variation during the growth of nucleus also implies the ranks of energies between different crystal surfaces. The sequential order between prism and second prism face also conform to the previous studies of surface energies and growing speed⁶⁵ and⁶⁶ that second prism face is of higher energy and entropy and growing slower than prism face, as in our results second prism face always emerge later and rarer than prism face. On the other hand, when prism face partially formed, instead of propagating in their normal directions, it is prior for nucleus to construct rest of prism faces to form hexagonal patterns, as we could see from alternating triangle/trapezoid and hex patterns in Fig. 6. The synchronization of prism faces represents similar energies of these symmetrical crystal face.



(a) Sandwich structure and equivalent face between Ih and Ic.



(b) Density distribution of nucleus in simulation.



(c) Density distribution of nucleus of standard Ih and Ic structure.

FIG. 8. Density plot and comparison of Ih and Ic morphology.

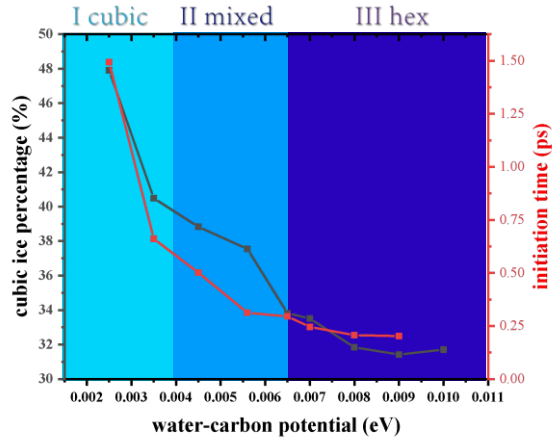
2. Similarity induced structure transition from Ih to Ic

Similarity and transition between 111 face of Ic and 100 face of Ih in structural symmetry, density profile is discovered and explained in our results. Fig. 8(a) is the stereoscopic nucleus shape in the case of $\epsilon = 0.45$ eV. Such sandwich structure of Ih and Ic alternating implies structure transition in the growth from Ih phase to Ic phase on the 100 face of Ih or 111 face of Ic as marked in Fig. 8(a), which suggests equivalence of 111 face in Ic and 001 in Ih. Further result of density distribution of Ic and Ih structures in the direction of axis proves existence of structural similarity. The density distribution of standard Ih and Ic structures nearly overlaps (Fig. 8(c)). Such similarity is also detected in density distribution plot (Fig. 8(b)) of nucleus formed in our simulations. The essence of this structural transformation is substituting axis bonds of hexagonal ice with symmetric bonds of cubic ice as we proved in method section and showed in Fig. 3(a). This collaborative transformation behavior of ice molecules leads to the configurational change of ice structures and phases. Such structure transformation dominated by similarity could well explain the preferential emergence of {001} faces of Ih and {111} faces of Ic in Sec. III A 1, as the {111} faces of Ic is prior to be induced by {001} face of Ih compared with other faces.

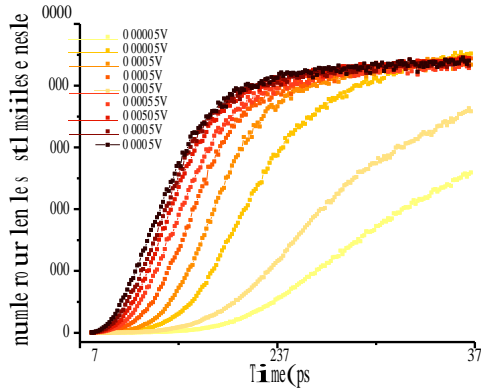
Transformation from Ih into Ic is also shown to prefer to start in the region of intersection part of edge of hexagonal ice and then extend to rest region of equivalent surface with tetrahedral shape consisting of 111 face and its symmetric counterparts, as Fig. 8(a) suggests.

B. Morphology variation of nucleus with different water-carbon potentials

As both structures of Ic and Ih tend to exhibit its own form of shape, morphology of nucleus in MD simulation is actually decided by relative contents of Ic and Ih. Definition of cubicity defined in method section is used to represent the relative contents and three morphological patterns produced by different water-carbon potentials are concluded. Morphological variation and nucleation pathway resulting in different morphology patterns of nucleus is also presented. Promotion of Ic structures with increasing nucleus size is discovered within nucleus spontaneity in nucleation process.



(a) Three distinct patterns. Cubicity and initiation time under all tested water-carbon potentials.



(b) Growth curve under all tested water-carbon potentials.

FIG. 9. Distinct patterns and growth curves.

1. Morphology patterns produced by different water-carbon potentials

Integral nucleus morphologies at different water-carbon surface energies could be categorized into three patterns as cubic pattern, mixed pattern and hex pattern of different cubicity marked in Fig. 9(a). At low surface energy region, the cubicity of nucleus is comparatively high (45% or higher), as Ih only exists in the vicinity of graphite surface, the stereo shape of nucleus is decided by Ic and exhibits tetrahedron shape of pyramids or shape of parallel pipe enclosed by 100 and 111 faces of Ic crystals as listed in Fig. 10. As surface energy increased, the portion of Ic declined (36-45%) and integral shape exhibits mixed shape of Ic tetrahedron stacked on Ih hexagonal prism. There are two distinct stackings in the mixed pattern (see in Fig. 10), which constructed by different upper part of Ic in the shape of tetrahedron or oblique prismoid and same hexagonal prism. When surface energy is rather high, the portion of Ic further decreases (33%-36%) and becomes fully attached to the hexagonal prism. The integral morphology is fully decided by Ih structures and exhibits shape of complete hexagonal prisms or fractal prisms as listed

in Fig. 10. Such hexagonal prism appears in all structure patterns as basal section as indicated.

Exhibition of three morphological patterns of an integral nucleus at different energy conditions is essentially different combination of Ic and Ih structures characterized by cubicity. Underlying nucleation pathways formulating different morphological patterns directed by different surface energies will be discussed in next section.

2. Morphology variation in nucleus growth process and nucleation pathway

Nucleus morphology also variates at different sizes in the nucleation process under different potential conditions. Fig. III B 2 of cubicity at different cluster sizes shows that cubicity of nucleus grows exponentially as nucleation proceeds and cluster size increases. (The cubicity used in the plot is averaged using nucleus identified of same sizes emerged in our simulations as cubicity may vibrate for different ice clusters.) Nucleus induced by substrate of different surface energies share a common structure homology of 10% cubicity structure and gradually diverges into different structures of different cubicity.

At primitive stage, nucleus grows up and gradually get free of fluctuation brought by thermal motions. The cubicity fluctuates around 10% at primitive stage of nucleus size smaller than 10, as circled in Fig. III B 2. As thermal fluctuation period marked in Fig. III B 2, the typical nucleus of 10% cubicity of ten molecules constructed of no hex rings is rather unstable to exist but repetitively emerging at different locations. Through tracing component molecules, same structure identified at different location is ascertained to be composed by different molecules, which proves that such fluctuation is not caused by molecules diffusion at the surface but thermal fluctuation. When nucleus grows into a size larger than 10, spatial structure of at least two connected rings is formed and stably adhering to the graphite surface. Such stabilization process of nucleus adhering to the graphite surface exist in the cases of all surface energies.

At stage of divergence, cubicity of nucleus formed under different energy conditions gradually diverges into different regions of cubic patterns, mixed patterns and hex patterns through different nucleation pathways. Nucleus formed under strong water-carbon energy conditions prefer to stretch along the surface and replicate its hexagonal rings structures of Ih, while nucleus under weak water-carbon surface energy conditions prefer to stretch upwards and replicate its cubic structures of Ic. The nucleus structures presented in same column of Fig. III B 2 of nucleation pathway is of the same size but different shape. Different tendencies in growth structures (Ih/Ic) lead to divergence in cubicity and eventually formation of different morphological patterns of nucleus. As presented in Fig. III B 2, cubicity of nucleus of 200-500 molecules at different energy conditions is distributed from 31% to 48%, which corresponds to different morphological patterns concluded in Fig. 9(a).

A spontaneous promotion of Ic structures by increasing nu-


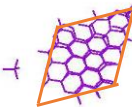
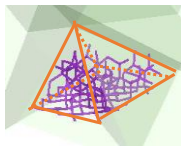
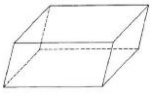

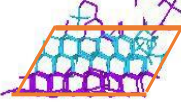
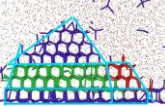
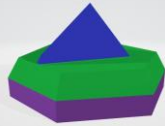
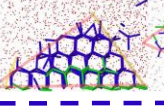
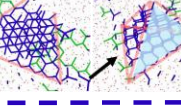
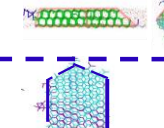
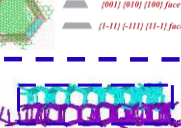

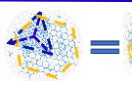

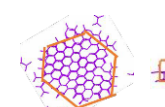
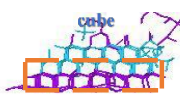
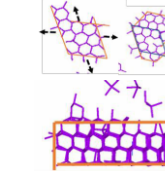
Pyramid	Side face: > {100} and {010} of Ic > {111} and {11-1} of Ic Basal face : > {001} of Th <div style="border: 1px solid black; padding: 2px; text-align: center;">Cubic Pattern</div>		Slice View Axis view	 
Parallel pipe	Side Crystal face: > {100} and {111} of Ic Basal face : > {001} of Th Top face > {001} of Th		Slice View Axis view	 
Mixed I	Top: Ic > Bottom face {111} > Side face {100} {010} {001} Mid: Ic > Bottom and top face {111} > Side face: six faces Bottom: > Bottom and top face {0001} > Side face: six side faces of prism <div style="border: 1px solid black; padding: 2px; text-align: center;">Mixed Pattern</div>	 	Top (mixed) Mid (Ic) Bottom (Ic)	   
Mixed II	Top: > Ic Tetrahedron enclosed by {111} {1-11} {11-1} {-111} Bottom: Th prism		Bottom (Ih)	 
normal prism	Two layers Ih and one layer Ic attached with Ih ice forming prism shape <div style="border: 1px solid black; padding: 2px; text-align: center;">Hex Pattern</div>		3-layer Prism base prevalent in three growing patterns 	
Fractal prism	Such prism tend to fragment into smaller prisms at some interfaces			

FIG. 10. Different patterns and structure details.

nucleus size is discovered from similarities in different nucleation pathways. Cubicity plot with nucleus size of Fig. III B 2 indicates that increase of Ic proportion in the nucleus is inevitable as molecules in the nucleus multiplies, despite of changes of water-carbon potentials. Growth curves under different water-carbon surface energy conditions show no essential differences apart from slightly variance in slopes, which suggests that multiply of cubic structure with nucleus size is the spontaneous behavior of nucleus growth instead of driven by surface heterogeneity. Reversely, strengthening of heterogeneity strength (water-carbon surface energy) delays such growth tendency of Ic structure as cubicity is declining with increase of water-carbon potentials in Fig. 9(a) and slope of cubicity in also declining with increase of water-carbon potentials in Fig. III B 2, which implies the existence of adverse

growth tendency brought by heterogeneity in nucleus growth.

Divergence of nucleation pathways shows a suppression of Ic structures under stronger surface energy, directing nucleus into different pathways leading to different morphological patterns concluded. Different nucleation pathways taken by nucleus of cubicity varied from 33% to 48% accords with the result of three morphological patterns and respective cubicity proposed in Sec. III B. Decline in cubicity while surface energy is increased illustrates that formation of Ic structures in nucleation is suppressed by strengthened surface energy. Only Ih structure is promoted by increased surface energy. Morphological variation concluded in Sec. III B 1 is the accumulative result of different surface affinities to Ic/Ih structures modulated by different surface energies, and such accumulation will finally switch different patterns on.

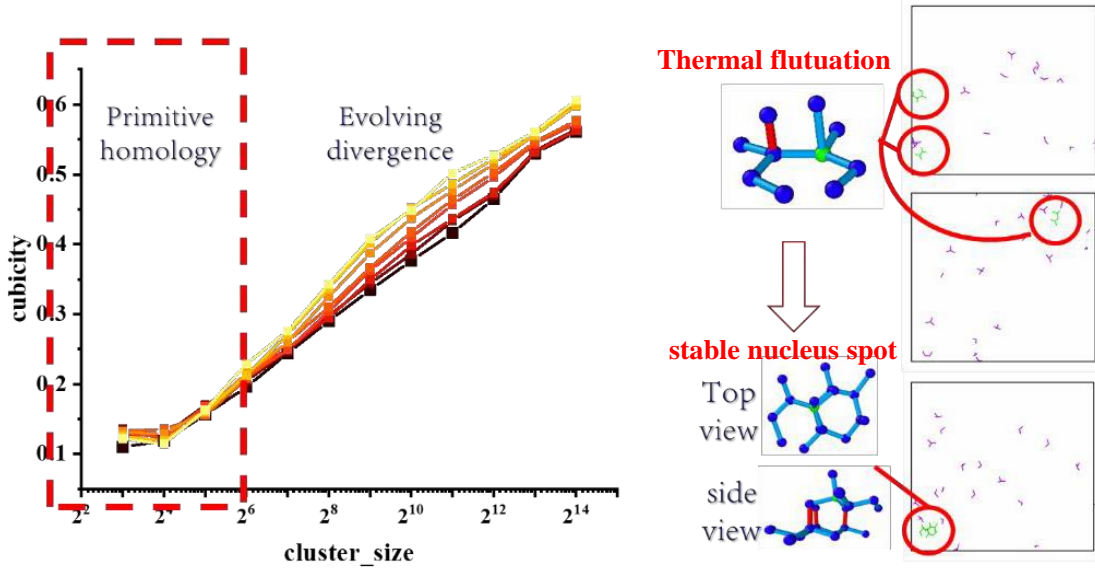


FIG. 11. Homology of structures under all tested water-carbon potentials and thermal fluctuation.

In summary, morphological variation during nucleation process could also be fully characterized and categorized using cubicity. An inherent promotion of Ic structures by increasing nucleus size is discovered from cubicity curves. Divergence of nucleation pathways accords with former concluded morphological patterns and respective cubicity. Morphological variation concluded in Sec. III B 1 is the accumulative result of different nucleation pathways caused by different surface affinities to Ic/Ih structures mediated by different surface energies.

C. Influence of pristine nucleus morphology and surface energy on subsequent nucleation process

Counteraction of pristine morphology on subsequent nucleus growth is investigated using seed method by inserting pristine nucleus onto surfaces of different water-carbon energies. Pristine nucleus of 60 molecules generated under 0.007 eV is chosen to be deployed onto surfaces of different energies to explore its variation from original nucleation pathways. Cubicity curves and growth curves are plotted to quantitatively measure deviation brought by change of pristine morphology.

1. Influence of pristine nucleus morphology on cubicity and nucleation pathway

Cubicity curve of seed method compared with curves under original 0.007 eV and 0.002 eV clearly clarifies the transition of structural cubicity from cubicity belonging to hex pattern under 0.007 eV to cubicity belonging to cubic pattern under 0.002 eV. Result of the curve is averaged from simu-

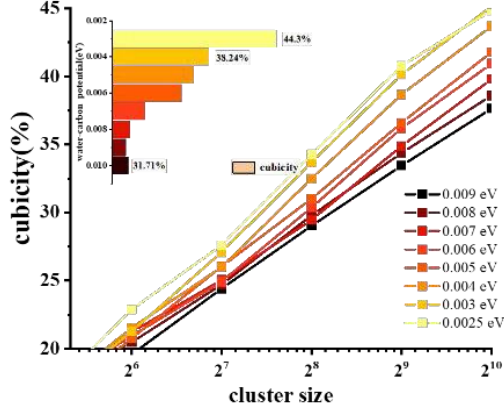
lations inserting nucleus generated under 0.007 eV to 0.002 eV with different initial velocity seed. The increase of cubicity is weakened at very beginning that the slope of the curve transverses under the original curve under 0.002 eV and 0.007 eV. After short period of a low origin point, the seed curve gradually threads from the curve under 0.007 eV to 0.002 eV, namely from the curve that generates the pristine nucleus to the curve of new surface energy.

The low slopes of starting period are caused by low cubicity of seeded structure and low Ic tendency brought within its spontaneity. Separated from the strong inductive environment of original 0.007 eV, the seed structure is freed to grow at even lower cubicity than cubicity under 0.007 eV but higher cubicity than itself as there exists expanding tendency of Ic in spontaneity. Such impairment to cubicity could also be observed in seeding result under other potentials except restarting original simulations at 0.007 eV as presented in Fig. 14.

Curve crossing from results under 0.007 eV to 0.002 eV of Fig. 14(a) shows that structural dominance transfers from Ih to Ic. As nucleation pathway exhibited in Fig. 13(a), nucleus smaller than 550 molecules is in the same hex pattern of fractal hexagonal prism grown under 0.007 eV. The hex pattern gradually transforms into mixed pattern at nucleus size of 1001 molecules which is combined with bottom hex prism and upper cubic oblique prismoid. At about 2000 molecules size nucleus finally evolves into cubic pattern which is in the same shape of parallel pipe listed in Fig. 10 in Sec. III B.

Dominance transformation from Ih to Ic exemplifies the process of spontaneous growth tendency inherently decided by structural component of present nucleus being gradually inverted by heterogeneity effect of surface energy. Low starting point and hex pattern exhibited affirm the spontaneous growth tendency brought with nucleus generated under 0.007

divergence with verified W-C strength



Nucleation pathway

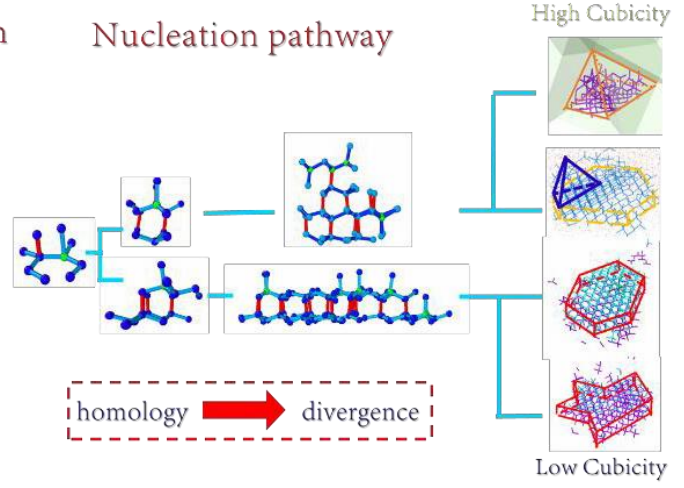


FIG. 12. Divergence of different structures of different cubicities under different nucleation pathways.

eV. Subsequent twisting in cubicity curve and transition showed in nucleation pathway validates the surface effect on nucleus morphology. Such detachment with original curve and pattern under 0.007 *eV* towards new potential all happens at about 512 molecules size. The final coincidence of cubicity curve and cubic morphology with original result under 0.002 *eV* prove the ultimate dominance of surface heterogeneity effect over nucleus morphology. Weakening surface energy tend to increase cubicity while strengthening surface energy tend to decrease cubicity. In summary, pristine morphology of nucleus is of limited influence on subsequent nucleus morphology after nucleus size grows into certain size. Surface heterogeneity effect has absolute dominance over ultimate nucleus morphology and decrease structure cubicity as it strengthens (increase cubicity as it weakens).

2. Influence of pristine nucleus morphology on growth curve

Growth curves of seed nucleus under different potential environment are compared with original curves under the same potential in Fig. 15. Nearly all curves are only translations of original curves which shortens the initiation time but leave the growth speed unchanged. Such curve gradually moves towards original curve under different potentials with potential difference decreased and finally overlaps with it as seed nucleus is excerpted from 0.007 *eV*.

Such translation of curves illustrates that growth speed in nucleation process is only decided by surface potentials and not influenced by pristine morphology of nucleus. The invariant growth speed represents the influence of surface energy and gradually modifies the nucleus cubicity and morphology into values decided by surface energy, which verifies former analyzed pattern transformation in last section. Growth speed could be used to represent the accumulative effect of surface

energy on nucleus morphology.

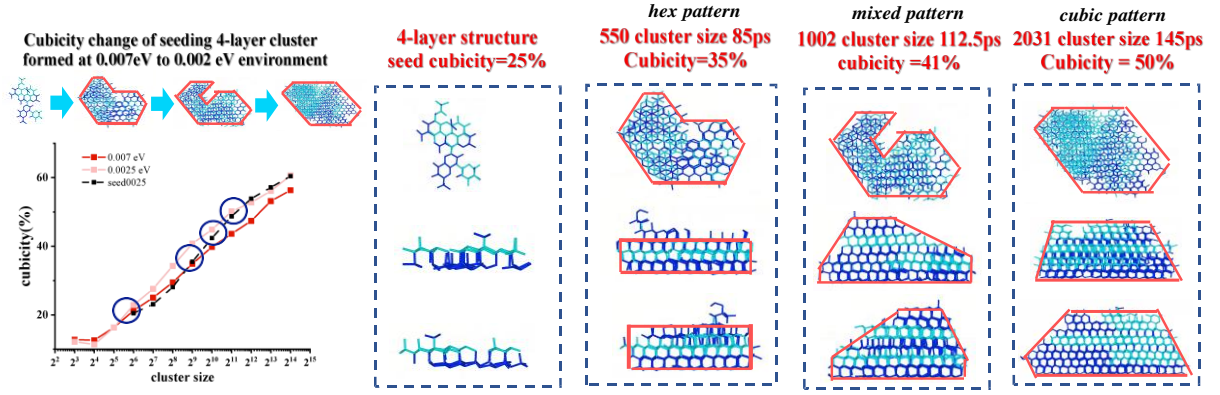
In summary, different pristine morphologies have no effect on growth speed and the ultimate morphology of nucleus. Growth speed in nucleation process is only decided by surface potentials and could be used to represent the accumulative effect of surface energy on nucleus morphology.

IV. CONCLUSION

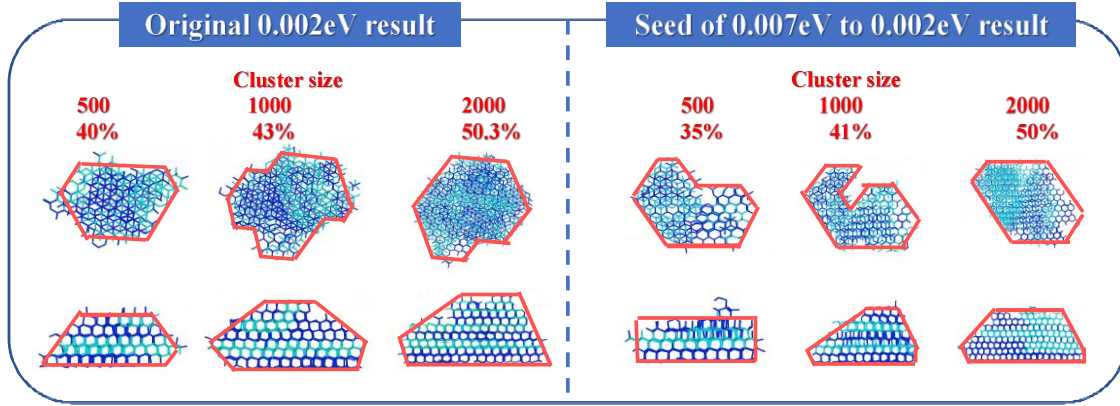
In this paper, a new algorithm for identifying ice nucleus is designed to give an explicit portrait of nucleus growth in MD simulations. The underlying symmetry requirement of traditional methods was exposed and utilized in distinguishing different crystal structures in this new algorithm, which enabled morphological studies for ice growth in microscopic simulations. Graphite surface was chosen to induce ice as it is one of the most investigated substrate materials in heterogeneous icing and easy to find comparisons. Low temperature is used to accelerate nucleation process for direct calculation of nucleation rate. Morphologies and contents of ice induced by graphite surface were inspected in detail to elucidate heterogeneity effect.

Morphologies of Ih and Ic structures extracted from ice nucleus surprisingly accords with macroscopic hex-shape and cubic-shape anisotropy. The transformation of these two structures is induced by the similarities in bond symmetries and density distribution between 111 crystal face of Ic and 100 crystal face of Ih.

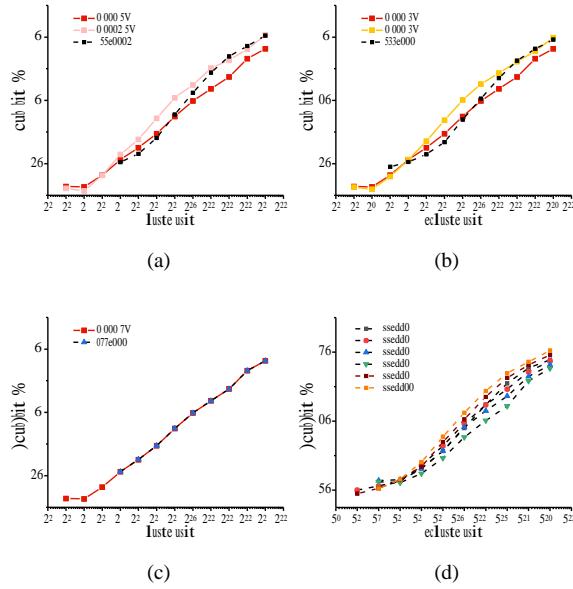
Three distinct morphological patterns and possible nucleation pathways of nucleus in simulations under different surface energies are concluded by analyzing constitutions of Ih and Ic structures contained. Morphological variation during nucleation process could also be fully characterized and categorized using cubicity. An inherent promotion of Ic structures



(a) Cubicity curve and nucleation pathway of seeded nucleus.



(b) Nucleus morphology comparison between seeded result and original result.

FIG. 13. Morphology influence on cubicity and nucleation pathway.**FIG. 14.** Cubicity curves of seeded result under different water-carbon potentials.

by increasing nucleus size is discovered from similarities in different nucleation pathways. Divergence of nucleation pathways shows a suppression of Ic structures under stronger surface energy, directing nucleus into different pathways leading to different morphological patterns concluded.

Pristine morphology is discovered of limited influence on the subsequent nucleation process. The ultimate cubicity and morphology are only decided by surface energy. The growth rate of ice nucleus is proved to be only decided by exterior factor of surface energy instead of interior factor of nucleus structures/constitutions with seed simulation initiated by different structured pristine nucleus. The ultimate cubicity decreases with increasing surface energy, showing a negative tendency in cubic structure growth.

The improved identification algorithm specialized by this paper is capable of giving insightful analysis into morphological behaviors of nucleation, which is meaningful for future researches on nucleus morphology using MD method. The surface energy effect and nucleation pathways discovered in this paper on nucleus in heterogeneous nucleation are fundamental to understand nucleation theory and ice morphological phenomenon in different scales.

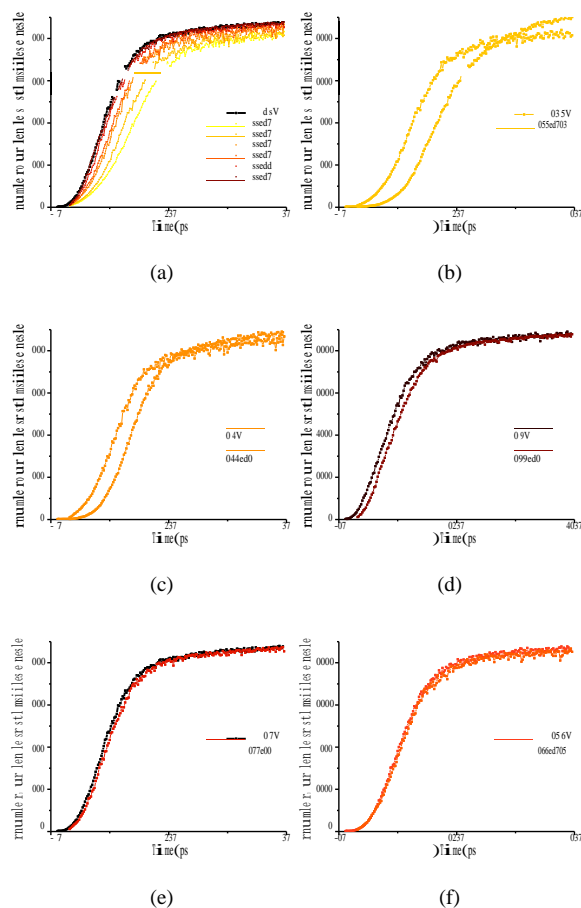


FIG. 15. Growth curves of seeded result under different water-carbon potentials.

ACKNOWLEDGMENT

This work was supported by the NSFC-DFG Mobility programme between Beihang University and Technical University of Munich (No. M - 0368) and the Integrated Projects utilizing the Space Environment on ISS and CSS supported by CMSA and ESA (No. TGMTYY00-RW-03).

- ¹H. H. Kieffer, P. R. Christensen, and T. N. Titus, "CO₂ jets formed by sublimation beneath translucent slab ice in Mars' seasonal south polar ice cap," *Nature* **442**, 793–796 (2006).
- ²I. V. Polyakov, L. A. Timokhov, V. A. Alexeev, S. Bacon, I. A. Dmitrenko, L. Fortier, I. E. Frolov, J.-C. Gascard, E. Hansen, V. V. Ivanov, S. Laxon, C. Mauritzen, D. Perovich, K. Shimada, H. L. Simmons, V. T. Sokolov, M. Steele, and J. Toole, "Arctic ocean warming contributes to reduced polar ice cap," *Journal of Physical Oceanography* **40**, 2743–2756 (2010).
- ³O. Parent and A. Ilinca, "Anti-icing and de-icing techniques for wind turbines: Critical review," *Cold regions science and technology* **65**, 88–96 (2011).
- ⁴W. Pike, "Extreme warm frontal icing on 25 February 1994 causes an aircraft accident near Uttoxeter," *Meteorological Applications* **2**, 273–279 (1995).
- ⁵Y. Cao, W. Tan, and Z. Wu, "Aircraft icing: An ongoing threat to aviation safety," *Aerospace science and technology* **75**, 353–385 (2018).
- ⁶S. Nickovic, B. Cvetkovic, S. Petkovic, V. Amiridis, G. Pejanovic, S. Solo-

- mos, E. Marinou, and J. Nikolic, "Cloud icing by mineral dust and impacts to aviation safety," *Scientific reports* **11**, 1–9 (2021).
- ⁷T. Cebeci and F. Kafyeke, "Aircraft icing," *Annual review of fluid mechanics* **35**, 11 (2003).
- ⁸A. R. Solangi, *Icing effects on power lines and anti-icing and de-icing methods*, Master's thesis, UiT The Arctic University of Norway (2018).
- ⁹M. Farzaneh, C. Volat, and A. Leblond, "Anti-icing and de-icing techniques for overhead lines," in *Atmospheric icing of power networks* (Springer, 2008) pp. 229–268.
- ¹⁰A. K. Andersson and L. Chapman, "The impact of climate change on winter road maintenance and traffic accidents in west midlands, uk," *Accident Analysis & Prevention* **43**, 284–289 (2011).
- ¹¹A. Andreasson, N. B. Kiss, C. C. Juhlin, and A. Höög, "Long-term storage of endocrine tissues at -80 °C does not adversely affect RNA quality or overall histomorphology," *Biopreservation and biobanking* **11**, 366–370 (2013).
- ¹²A. Glushakova and A. Kachalkin, "Endophytic yeasts in *Malus domestica* and *Pyrus communis* fruits under anthropogenic impact," *Microbiology* **86**, 128–135 (2017).
- ¹³X. Liu, "Heterogeneous nucleation or homogeneous nucleation?" *The Journal of Chemical Physics* **112**, 9949–9955 (2000).
- ¹⁴K. K. Varanasi, M. Hsu, N. Bhate, W. Yang, and T. Deng, "Spatial control in the heterogeneous nucleation of water," *Applied Physics Letters* **95**, 094101 (2009).
- ¹⁵Z. Zhang and X.-Y. Liu, "Control of ice nucleation: freezing and antifreeze strategies," *Chemical Society Reviews* **47**, 7116–7139 (2018).
- ¹⁶P. A. Muñoz, S. L. Márquez, F. D. González-Nilo, V. Márquez-Miranda, and J. M. Blamey, "Structure and application of antifreeze proteins from antarctic bacteria," *Microbial cell factories* **16**, 1–13 (2017).
- ¹⁷L. Fay and X. Shi, "Environmental impacts of chemicals for snow and ice control: state of the knowledge," *Water, Air, & Soil Pollution* **223**, 2751–2770 (2012).
- ¹⁸M. Fitzner, G. C. Sosso, S. J. Cox, and A. Michaelides, "The many faces of heterogeneous ice nucleation: Interplay between surface morphology and hydrophobicity," *Journal of the American Chemical Society* **137**, 13658–13669 (2015).
- ¹⁹Y. Zhao, Q. Guo, T. Lin, and P. Cheng, "A review of recent literature on icing phenomena: Transport mechanisms, their modulations and controls," *International Journal of Heat and Mass Transfer* **159**, 120074 (2020).
- ²⁰S. Nath, S. F. Ahmadi, and J. B. Boreyko, "A review of condensation frosting," *Nanoscale and Microscale Thermophysical Engineering* **21**, 81–101 (2017).
- ²¹D. Tian, Y. Song, and L. Jiang, "Patterning of controllable surface wettability for printing techniques," *Chemical society reviews* **42**, 5184–5209 (2013).
- ²²R. Cabriolu and T. Li, "Ice nucleation on carbon surface supports the classical theory for heterogeneous nucleation," *Physical Review E* **91**, 052402 (2015).
- ²³Q. Zeng and S. Xu, "Thermodynamics and characteristics of heterogeneous nucleation on fractal surfaces," *The Journal of Physical Chemistry C* **119**, 27426–27433 (2015).
- ²⁴T. Li, D. Donadio, G. Russo, and G. Galli, "Homogeneous ice nucleation from supercooled water," *Physical Chemistry Chemical Physics* **13**, 19807–19813 (2011).
- ²⁵Y. Djikaev and E. Ruckenstein, "Self-consistent determination of the ice–air interfacial tension and ice–water–air line tension from experiments on the freezing of water droplets," *The Journal of Physical Chemistry C* **121**, 16432–16439 (2017).
- ²⁶P. Eberle, M. K. Tiwari, T. Maitra, and D. Poulikakos, "Rational nanostructuring of surfaces for extraordinary icephobicity," *Nanoscale* **6**, 4874–4881 (2014).
- ²⁷C. Li, Z. Liu, E. C. Goonetilleke, and X. Huang, "Temperature-dependent kinetic pathways of heterogeneous ice nucleation competing between classical and non-classical nucleation," *Nature communications* **12**, 1–9 (2021).
- ²⁸Y. Bi, B. Cao, and T. Li, "Enhanced heterogeneous ice nucleation by special surface geometry," *Nature communications* **8**, 1–7 (2017).
- ²⁹K. G. Libbrecht, "Physical dynamics of ice crystal growth," *Annu. Rev. Mater. Res.* **47**, 271–295 (2017).
- ³⁰V. I. Kalikmanov, "Classical nucleation theory," in *Nucleation theory* (Springer, 2013) pp. 17–41.
- ³¹D. Richard and T. Speck, "Classical nucleation theory for the crystallization

- kinetics in sheared liquids,” *Physical Review E* **99**, 062801 (2019).
- ³²M. A. Holden, J. M. Campbell, F. C. Meldrum, B. J. Murray, and H. K. Christenson, “Active sites for ice nucleation differ depending on nucleation mode,” *Proceedings of the National Academy of Sciences* **118**, e2022859118 (2021).
 - ³³N. Saleema, M. Farzaneh, R. W. Paynter, and D. K. Sarkar, “Prevention of ice accretion on aluminum surfaces by enhancing their hydrophobic properties,” *Journal of adhesion science and technology* **25**, 27–40 (2011).
 - ³⁴J. Liu, C. Zhu, K. Liu, Y. Jiang, Y. Song, J. S. Francisco, X. C. Zeng, and J. Wang, “Distinct ice patterns on solid surfaces with various wettabilities,” *Proceedings of the National Academy of Sciences* **114**, 11285–11290 (2017).
 - ³⁵Y. Djikaev, A. Tabazadeh, P. Hamill, and H. Reiss, “Thermodynamic conditions for the surface-stimulated crystallization of atmospheric droplets,” *The Journal of Physical Chemistry A* **106**, 10247–10253 (2002).
 - ³⁶N. H. Fletcher, “Size effect in heterogeneous nucleation,” *The Journal of chemical physics* **29**, 572–576 (1958).
 - ³⁷X. Y. Liu and J. De Yoreo, *Nanoscale Structure and Assembly at Solid-fluid Interfaces: Assembly in hybrid and biological systems*, Vol. 2 (Springer Science & Business Media, 2004).
 - ³⁸V. Tatarchenko, *Shaped crystal growth*.
 - ³⁹T. O. Drews, M. A. Katsoulakis, and M. Tsapatsis, “A mathematical model for crystal growth by aggregation of precursor metastable nanoparticles,” *The Journal of Physical Chemistry B* **109**, 23879–23887 (2005).
 - ⁴⁰D. Rozmanov and P. G. Kusalik, “Anisotropy in the crystal growth of hexagonal ice, *ice Ih*,” *The Journal of chemical physics* **137**, 094702 (2012).
 - ⁴¹Y. Teraoka, A. Saito, and S. Okawa, “Ice crystal growth in supercooled solution,” *International Journal of Refrigeration* **25**, 218–225 (2002).
 - ⁴²G. C. Sosso, J. Chen, S. J. Cox, M. Fitzner, P. Pedevilla, A. Zen, and A. Michaelides, “Crystal nucleation in liquids: Open questions and future challenges in molecular dynamics simulations,” *Chemical reviews* **116**, 7078–7116 (2016).
 - ⁴³D. Gebauer, M. Kellermeier, J. D. Gale, L. Bergström, and H. Cölfen, “Pre-nucleation clusters as solute precursors in crystallisation,” *Chemical Society Reviews* **43**, 2348–2371 (2014).
 - ⁴⁴C. Gurganus, A. B. Kostinski, and R. A. Shaw, “Fast imaging of freezing drops: No preference for nucleation at the contact line,” *The Journal of Physical Chemistry Letters* **2**, 1449–1454 (2011).
 - ⁴⁵Q. Guo and P. Cheng, “Numerical investigations of six-fold dendritic icing process in subcooled water subject to natural and forced convective environments,” *International Journal of Heat and Mass Transfer* **145**, 118658 (2019).
 - ⁴⁶L. S. Bartell and D. T. Wu, “Do supercooled liquids freeze by spinodal decomposition?” *The Journal of chemical physics* **127**, 174507 (2007).
 - ⁴⁷T. Kim and M. C. Lin, “Visual simulation of ice crystal growth,” in *Proceedings of the 2003 ACM SIGGRAPH/Eurographics symposium on Computer animation* (Citeseer, 2003) pp. 86–97.
 - ⁴⁸M. Schäfer, E. Bierwirth, A. Ehrlich, F. Heyner, and M. Wendisch, “Retrieval of cirrus optical thickness and assessment of ice crystal shape from ground-based imaging spectrometry,” *Atmospheric Measurement Techniques* **6**, 1855–1868 (2013).
 - ⁴⁹W. Kong and H. Liu, “A theory on the icing evolution of supercooled water near solid substrate,” *International Journal of Heat and Mass Transfer* **91**, 1217–1236 (2015).
 - ⁵⁰M. Schremb and C. Tropea, “Solidification of supercooled water in the vicinity of a solid wall,” *Physical review E* **94**, 052804 (2016).
 - ⁵¹A. Criscione, I. Roisman, S. Jakirlic, and C. Tropea, “Towards modelling of initial and final stages of supercooled water solidification,” *International Journal of Thermal Sciences* **92**, 150–161 (2015).
 - ⁵²A. P. Thompson, H. M. Aktulga, R. Berger, D. S. Bolintineanu, W. M. Brown, P. S. Crozier, P. J. in’t Veld, A. Kohlmeyer, S. G. Moore, T. D. Nguyen, *et al.*, “Lammps—a flexible simulation tool for particle-based materials modeling at the atomic, meso, and continuum scales,” *Computer Physics Communications* **271**, 108171 (2022).
 - ⁵³P. Rein ten Wolde, M. J. Ruiz-Montero, and D. Frenkel, “Numerical calculation of the rate of crystal nucleation in a Lennard-Jones system at moderate undercooling,” *The Journal of chemical physics* **104**, 9932–9947 (1996).
 - ⁵⁴A. H. Nguyen and V. Molinero, “Identification of clathrate hydrates, hexagonal ice, cubic ice, and liquid water in simulations: The chill+ algorithm,” *The Journal of Physical Chemistry B* **119**, 9369–9376 (2015).
 - ⁵⁵T. Li, D. Donadio, and G. Galli, “Nucleation of tetrahedral solids: A molecular dynamics study of supercooled liquid silicon,” *The Journal of chemical physics* **131**, 224519 (2009).
 - ⁵⁶S. Auer and D. Frenkel, “Numerical prediction of absolute crystallization rates in hard-sphere colloids,” *The Journal of chemical physics* **120**, 3015–3029 (2004).
 - ⁵⁷L. Lupi, A. Hudait, and V. Molinero, “Heterogeneous nucleation of ice on carbon surfaces,” *Journal of the American Chemical Society* **136**, 3156–3164 (2014).
 - ⁵⁸W. Humphrey, A. Dalke, and K. Schulten, “Vmd: visual molecular dynamics,” *Journal of molecular graphics* **14**, 33–38 (1996).
 - ⁵⁹V. Molinero and E. B. Moore, “Water modeled as an intermediate element between carbon and silicon,” *The Journal of Physical Chemistry B* **113**, 4008–4016 (2009).
 - ⁶⁰R. Vink, G. Barkema, W. Van der Weg, and N. Mousseau, “Fitting the stillinger–weber potential to amorphous silicon,” *Journal of non-crystalline solids* **282**, 248–255 (2001).
 - ⁶¹A. Adamson and A. Gast, “Wiley interscience publication,” *Physical Chemistry of Surfaces*, John Wiley & Sons, Inc., New York (1997).
 - ⁶²H. Li and X. C. Zeng, “Wetting and interfacial properties of water nanodroplets in contact with graphene and monolayer boron–nitride sheets,” *ACS nano* **6**, 2401–2409 (2012).
 - ⁶³Q. Spreiter and M. Walter, “Classical molecular dynamics simulation with the velocity verlet algorithm at strong external magnetic fields,” *Journal of Computational Physics* **152**, 102–119 (1999).
 - ⁶⁴D. J. Evans and B. L. Holian, “The nose–hoover thermostat,” *The Journal of chemical physics* **83**, 4069–4074 (1985).
 - ⁶⁵J. Espinosa, C. Vega, and E. Sanz, “The mold integration method for the calculation of the crystal–fluid interfacial free energy from simulations,” *The Journal of chemical physics* **141**, 134709 (2014).
 - ⁶⁶J. R. Espinosa, C. Vega, and E. Sanz, “Ice–water interfacial free energy for the tip4p, tip4p/2005, tip4p/ice, and mw models as obtained from the mold integration technique,” *The Journal of Physical Chemistry C* **120**, 8068–8075 (2016).